

Ultrasonic-attenuation determination of the anisotropic energy gap in superconducting zinc*

C. R. Cleavelin and B. J. Marshall

Department of Physics, Texas Tech University, Lubbock, Texas 79409

(Received 24 January 1974)

Measurements of the ultrasonic attenuation in normal and superconducting high-purity zinc single crystals have been conducted for longitudinal sound waves propagating in the [0001], [1010], and [1120] crystallographic directions. Analysis of the data has been presented in terms of the BCS theory of superconductivity and the Pippard theory of ultrasonic attenuation. The analysis indicates the effective 0-K energy gap is highly anisotropic ($\langle a^2 \rangle \approx 0.04$). The analysis also indicates multiple-gap and frequency-dependent behavior of the energy gap for ultrasound propagating in the [1010] and [1120] directions for $ql \sim 1$. For zinc, this behavior has been attributed to anisotropy on the Fermi surface and not to multiple energy surfaces occurring in the higher Brillouin zones.

I. INTRODUCTION

In previous low-temperature ultrasonic-attenuation measurements¹⁻³ in pure zinc, the anisotropy in the superconducting energy gap was indicated to be no larger than $\pm 5\%$. However, a much larger anisotropy has been suggested by measurements of thermal conductivity,⁴ electronic specific heat,^{5,6} depression of the transition temperature T_c by non-magnetic impurities,⁷ microwave absorption,⁸ and recently by critical-field measurements.⁹ The mean anisotropy that has been suggested by these measurements is found to be as large as 22% ($\langle a^2 \rangle = 0.047$).

In the measurements of Farrell, Park, and Coles⁷ in the variation of T_c in zinc-based alloys and also in the measurements of Ducla-Soares and Cheeke⁵ on the electronic specific heat of zinc, both groups used a simple two-gap model, first suggested by Cooper,¹⁰ where they assumed that the energy gap over one region of the Fermi surface differed from the energy gap over the rest of the surface. Specifically, Farrell *et al.* suggested that the electron-electron interaction potential $V(\vec{k}, \vec{k}')$ near the c axis was much larger than that associated with most of the Fermi surface. This same interpretation of anisotropy of the energy gap was found consistent with the microwave absorption experiments of Evans, Garfunkel, and Hays.⁸ It is therefore the intent of the present study to resolve the discrepancies between the ultrasonic determinations and the other aforementioned determinations of the anisotropy in the energy gap in zinc.

II. EXPERIMENTAL

The high-purity zinc single crystal used in these measurements was obtained from Materials Research Corporation¹¹ (MRC). MRC certified that this crystal was grown from 99.9999% pure zinc. A smaller crystal was machined from the original crystal with an Elox TQH-31 electric-discharge machine. Since zinc has a hexagonal-close-packed (hcp) structure, the three independent crystallo-

graphic directions chosen for this study were the [0001] (c axis), [1010], and [1120] directions. Since each of these three axes is at an angle of 90° with respect to the other two, it was therefore possible to make all of the ultrasonic measurements on one zinc sample in the form of a rectangular parallelepiped with the approximate dimensions $4.2 \times 5.8 \times 7.9$ mm. In order to identify and estimate the accuracy of the orientation of these crystallographic axes during the machining process, the well-known Laue back-reflection technique¹² was employed. During the preparation of the zinc sample, it was observed in the Laue photographs that small surface irregularities were produced by the spark machining. These irregularities were subsequently removed by etching the sample in (3-4)% concentrated nitric acid in methanol. After the etching procedure, the sample was again x rayed and each pair of opposite end faces was measured for parallelism. It was found that each pair of end faces had a deviation of less than 1° from their respective principle lattice planes and that each pair was parallel to within 0.0005 cm over their entire surfaces.

In most conventional ultrasonic-attenuation measuring systems,¹³ measurements of less than 1 dB are normally prohibitive due to small signal-to-noise ratios. To overcome this difficulty, the system employed in these measurements utilizes sampling integration and phase-sensitive detection for enhancement of the signal-to-noise ratio in the amplification of the echoes. A block diagram of the complete ultrasonic system is shown in Fig. 1.

Since the detailed operation of this ultrasonic system has been reported elsewhere,¹⁴ only a brief description of the system will be given in this paper. The ultrasonic system consisted of essentially three independent subsystems: (i) the transmitting and receiving system, (ii) the display and recorder system, and (iii) the phase-detection system. The transmitter which produced the rf pulses was an Arenberg model No. PG-640C pulsed oscillator. A pulse width of 1-2 μ sec was used through-

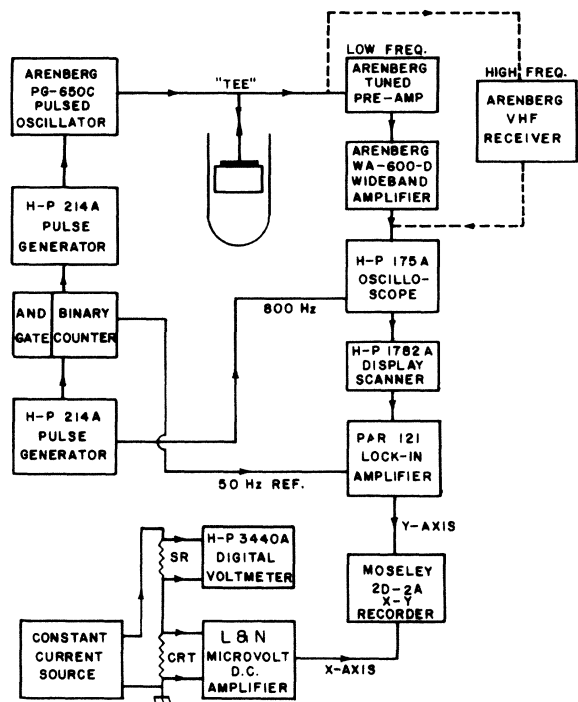


FIG. 1. Block diagram of the ultrasonic-attenuation and temperature-measurement systems.

out these measurements. The frequency of oscillation was tunable from about 0.5 MHz to approximately 225 MHz and the various frequencies were measured on a Hewlett-Packard 5245L electronic counter. For rf frequencies within the range 10–65 MHz the receiver system was an Arenberg model No. PA-620SN preamplifier and a model No. WA-600-D wide-band amplifier, while for the rf frequency range 55–210 MHz the receiver system was an Arenberg model No. VR-720 VHF receiver. After video amplification in either receiver system, the signal was then displayed on a Hewlett-Packard model No. 175A oscilloscope which was equipped with a Hewlett-Packard model No. 1782A display scanner.

The operation of the phase-detection system was to electronically chop the transmitter pulse repetition frequency (800 Hz) by chopping the transmitter triggering frequency at the fixed reference frequency of 50 Hz. Then, as the echo trains were received at the reference frequency, one echo was selected by means of sampling integration, i.e., using the display scanner in its manual mode of operation and sampling a point on the trace that corresponds to an acoustic echo peak. The resulting ac signal 50 Hz from the display scanner, which was proportional in amplitude to the amplitude of the echo and varying at the reference frequency, was sent to the Princeton Applied Research model

No. 121 lock-in amplifier. This signal was then detected at the reference frequency while discriminating against all other frequencies. The output voltage of the lock-in amplifier, which was directly proportional to the variation in echo height, was then displayed on the Y axis of the Moseley model No. 2D-2A X-Y recorder. The system was calibrated by simultaneously measuring an echo-height voltage change with a Tektronic type W comparator plug-in unit and reading the voltage change directly from the X-Y recorder.

In order to achieve and sustain sufficiently low temperatures in the study of superconducting zinc ($T_c = 0.84$ K), a conventional He³ evaporative refrigerator¹⁵ was utilized. The cryostat was specifically designed to incorporate an rf transmission line for the ultrasonic wave pulses. In its final configuration, the He³ refrigerator could sustain temperatures to the nearest millikelvin for approximately 10 h in the temperature range 1.5–0.37 K.

The primary temperature reference in these measurements was the He³ vapor pressure as measured by a precision Wallace and Tiernan model No. FA-160 absolute pressure gauge. The temperature of the He³ liquid and condensing can was determined by finding the corresponding temperatures and vapor pressures from the T_{62} He³ thermometry tables.¹⁶ In order to record the temperature variations on the X-Y recorder, secondary thermometers which gave dc voltages proportional to the temperature variations were employed. The thermometers used for this purpose were carbon resistance thermometers (CRT). For this study, two $\frac{1}{2}$ -W Allen-Bradley CRTs of different resistance (nominal room-temperature resistances of 5.1 and 2.7 Ω) were mounted in a pure copper stand which was in direct contact with the He³ condensing can and zinc specimen. To ensure good thermal contact between both CRTs and the copper mounting stand, the resistors were coated with Dow Corning DC-11 silicon grease before mounting them in the copper stand. The basic measuring method, the well-known four-terminal method, is seen in Fig. 1. During data taking, a constant current of 1.000 μ A was used, and the CRT output voltage was amplified by a Leeds and Northrup model No. 9835-B dc microvolt amplifier and then displayed on the X axis of the X-Y recorder. The CRTs were recalibrated against the He³ vapor pressure each time the He³ refrigerator was recycled. In order to interpolate between the calibration points and to extend the resistance-versus-temperature data to 0.37 K, the calibration data were fitted using a least-squares method to the Clement-Quinnell equation.¹⁷

The pulse-echo technique required that a rigid uniform bond exist between the quartz wafer transducer and the zinc specimen. The most suitable bonding material that could be applied at room tem-

perature was found to be the DC-11 silicon grease previously mentioned.

III. ANALYSIS OF DATA

It is well known that one of the principal parameters determining the magnitude of ultrasonic attenuation due to the conduction electrons is the ratio of the ultrasound wavelength to the electron mean free path l . This is normally expressed as the product ql , where $q = 2\pi/\lambda$. Using a free-electron model for an isotropic metal, Pippard¹⁸ has shown that the over-all dependence of the longitudinal lattice wave attenuation on ql is given by

$$\alpha = \alpha' \frac{6}{\pi} \left(\frac{ql \tan^{-1}(ql)}{3[ql - \tan^{-1}(ql)]} - \frac{1}{ql} \right), \quad (1)$$

where α' is the limiting attenuation when $ql \gg 1$. For the regime $ql > 1$, Pippard's calculations yield an attenuation coefficient that varies linearly with frequency and is independent of ql :

$$\alpha = (\pi N m_e v_F / 6 \rho_0 v_s^2) \omega. \quad (2)$$

Here N is the number of electrons per unit volume, m_e is the mass of a free electron, ρ_0 is the density of the metal, v_s is the longitudinal wave velocity, v_F is the Fermi velocity, and ω is the angular frequency of the ultrasonic wave. In order to fit the total electronic attenuation data to Eq. (1), the limiting attenuation α' and the mean free path l have been left as adjustable parameters. The average mean free path determined in this manner is compared to that measured by a magnetoacoustic method to be discussed later.

For low-frequency longitudinal ultrasonic waves, BCS¹⁹ predict that the ratio of superconducting- to normal-state attenuation in the regime $ql > 1$ is given by

$$\alpha_s / \alpha_n = 2 / (e^{\Delta(T)/kT} + 1) = 2f(\Delta(T)), \quad (3)$$

where $\Delta(T)$ is the isotropic temperature-dependent energy gap. Tsuneto²⁰ has shown that this result holds equally well for all values of ql in the region of impurity-limited scattering. As has been invoked in previous ultrasonic studies, the form of Eq. (3) is assumed correct for an anisotropic superconductor. However, for each crystallographic direction studied, the limiting value of the energy gap $\Delta(\vec{q}, T)_{T=0}$ can assume a value different from the BCS value of $1.76kT_c$, where T_c is the transition temperature of the pure superconductor. In order to fit the attenuation data to Eq. (3) and determine the effective energy gap $\Delta(\vec{q}, 0)$, Eq. (3) was rewritten as

$$\ln[2(\alpha_n / \alpha_s) - 1] = [\Delta(\vec{q}, 0) / kT_c][G(t)/t], \quad (4)$$

where $G(t) = \Delta(T) / \Delta(0)$ for an ideal superconductor and $t = T / T_c$. The function $G(t)$ has been tabulated from the BCS theory by Muhlschlegel.²¹ However,

for purposes of calculation of the attenuation data, it was found more convenient to use an analytical form of $G(t)$ developed by Clem²²:

$$G(t) = 1.7367(1-t)^{1/2} \times [1 - 0.4095(1-t) - 0.0626(1-t^2)]. \quad (5)$$

This analytical form has been shown to reproduce Muhlschlegel's values for $G(t)$ with an error of less than 0.1% for $t > 0.4$.

Equation (4) suggests that a plot of $\ln[2(\alpha_n / \alpha_s) - 1]$ as a function of $G(t)/t$ should be a straight line whose slope is the effective energy gap at 0 K if the BCS theory gives a consistent description of the experimental data. It is also observed that this type of analysis gives allowance for the possibility of multiple energy gaps, since if more than one 0-K energy gap is present, the plot of Eq. (4) should deviate from a single slope fit.

In order to obtain the superconducting- to normal-state attenuation ratio α_s / α_n from the experimental data, it is necessary to isolate the nonelectronic attenuation so that the zero-point attenuation $\alpha_s(0)$, and therefore the total electronic attenuation α_e , can be determined. This was accomplished in the usual manner by treating $\alpha_s(0)$ as an adjustable parameter which best linearizes the experimental data consistent with Eq. (4). The computation of the experimental data was performed on an IBM 360/50 computer facility using the method of least squares where $\alpha_s(0)$ and $\Delta(0)$ were left as adjustable parameters. Since the fitting procedure allowed for multiple energy gaps (more than one slope), the computer program was written in such a manner that if more than one slope occurred in the fit, $\alpha_s(0)$ was varied until the best fit was obtained for the slope which occurred at the lower reduced temperatures. Then this value of $\alpha_s(0)$ was used to fit the slope or slopes occurring at the higher reduced temperatures. It was found that $\alpha_s(0)$ could always be estimated from the attenuation data for $t \leq 0.80$.

It should be noted that this type of experimental examination does not necessarily determine the functional form of $\alpha_s(T)$ uniquely, although it does provide experimental evidence for the consistency of the experimental observations with the BCS relation, Eq. (3). To emphasize this point, it has been observed for the four elemental superconducting materials zinc, cadmium, molybdenum, and lead studied in this laboratory that the following empirical relation also represents very well the functional form of the experimental data for $t < 0.80$:

$$\alpha_s / \alpha_n \propto t^3, \quad (6)$$

where t is the reduced temperature. Representations of the experimental data in this functional form are seen in Fig. 2.

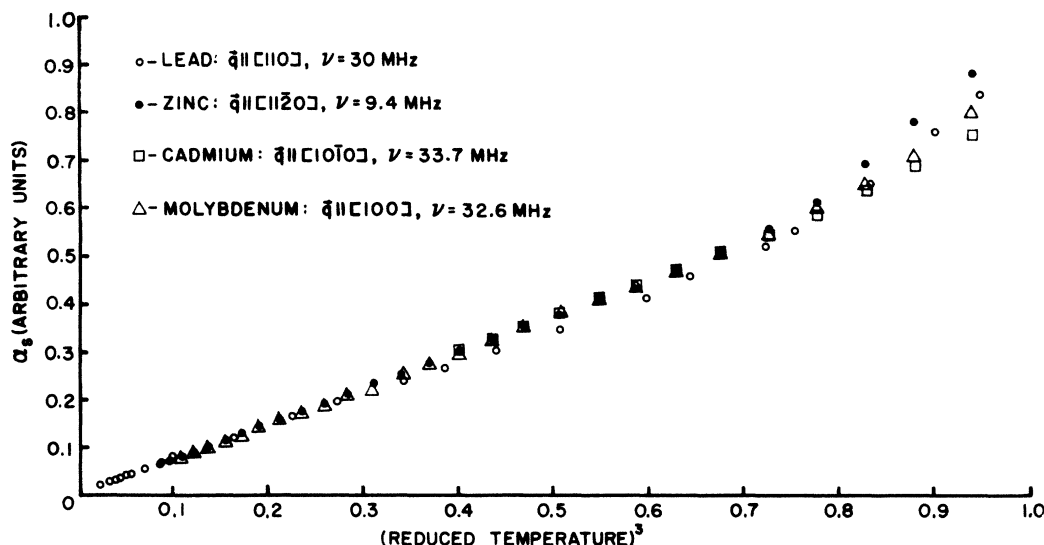


FIG. 2. Representations of the ultrasonic attenuation in the superconducting state for the four elemental superconductors lead, zinc, cadmium, and molybdenum vs the cube of the reduced temperature. The lead data were normalized by assuming the normal-state attenuation α_n was constant and equal to its value at the transition temperature.

Besides the directional dependence of the attenuation on ql , the nature of the ultrasonic measurement produces a selectivity in the interaction of the lattice wave with the electrons on the Fermi surface. This selectivity denotes the so-called "effective zone," i. e., it essentially indicates which electrons on the Fermi surface enter into the electron-phonon interaction causing the electronic attenuation of the ultrasonic wave. Leibowitz²³ has discussed the selectivity for the free-electron model in terms of the angle θ between the Fermi velocity \vec{v}_F and the sound-wave vector \vec{q} . He demonstrates that for $ql \geq 1$ the amplitude of the perturbation of the electron distribution due to the lattice waves falls to half-maximum when

$$\cos\theta \approx v_s/v_F + 1/ql. \quad (7)$$

This expression indicates that the electron-phonon selectivity is enhanced with the increase of ql and that the interaction is weighted toward the electrons having Fermi velocities perpendicular to the sound wave vector \vec{q} . As ql becomes much larger than unity and since $v_s/v_F \sim 10^{-3}$, Eq. (7) indicates that the "effective zone" becomes a very narrow band satisfying $\vec{v}_F \cdot \vec{q} \approx v_s$. This is the same result that Morse²⁴ originally arrived at by treating the electron-lattice interaction as a quantum-mechanical electron-phonon scattering process for $ql \gg 1$. Thus Eq. (7) suggests that for a highly anisotropic superconductor such as zinc, the energy gap and also the total electronic attenuation should depend on ql and that this dependency should vanish for $ql \rightarrow \infty$.

IV. EXPERIMENTAL RESULTS AND DISCUSSION

A. ql determination

It is evident from the discussion in Sec. III that an estimate of the mean free path is essential to the data interpretation since both the total electronic attenuation α_e and the energy gap $\Delta(\vec{q}, 0)$ are expected to be functions of ql . In this study, the zinc specimen was impurity limited below about 4 K. Therefore the functional dependence due to ql below 4 K should be determined by the magnitude of \vec{q} and the anisotropy of l over the "effective zone." Usually the average electron mean free path is estimated from residual resistivity measurements. However, this method gives no indication as to the anisotropy of the mean free path. Therefore a method which was proposed by Deaton and Gaven-da²⁵ and previously used by Deaton²⁶ in a study on zinc and cadmium was used for the mean-free-path determinations. This method is essentially a magnetoacoustic analysis of the high-magnetic-field attenuation of ultrasonic waves utilizing the free-electron model. Pippard²⁷ has shown that the limit of the attenuation in high magnetic fields is proportional to q^2l and that this limit is approached as $1/H^2$. It has also been shown in a numerical calculation²⁵ that the high-field-saturation attenuation is equal to the attenuation in zero field for $ql = 6.8$. Therefore the mean free path could be determined by plotting the difference between the high-field and zero-field attenuation as a function of frequency, thus determining the frequency where $ql = 6.8$. Anisotropy in the mean free path was determined by rotating the magnetic-field vector in

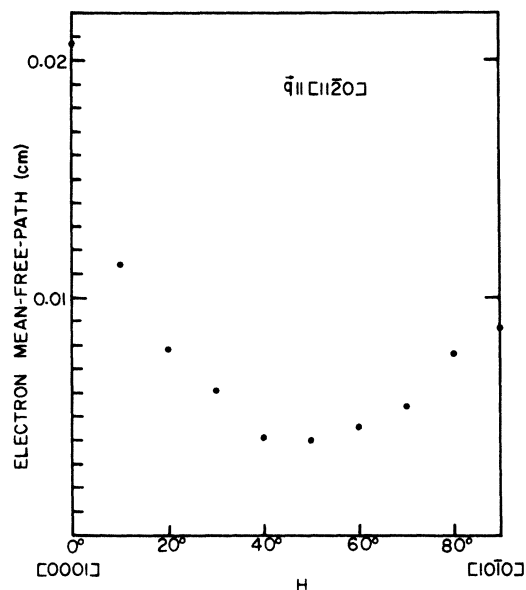


FIG. 3. Angular anisotropy of the high-field ultrasonic-attenuation data for zinc at $T = 1.42$ K.

a plane perpendicular to the sound wave vector. The results of this analysis were similar to those obtained in Deaton's study.²⁸ Shown in Fig. 3 are the results for the $[11\bar{2}0]$ crystallographic direction indicating the large anisotropy in the mean free path.

B. Superconducting- and normal-state attenuation results

Before the attenuation data could be analyzed, an accurate determination of the superconducting transition temperature for zinc was required. The transition temperature was determined in each crystallographic direction studied by observing at what temperature the attenuation abruptly changed from the normal to superconducting state and vice versa. Using this criterion, the transition temperature was determined to be 0.840 ± 0.005 K in all three crystallographic directions.

1. Results for $\vec{q} \parallel [0001]$

Shown in Fig. 4 are plots of $\ln[2(\alpha_n/\alpha_s) - 1]$ as a function of $G(t)/t$ at frequencies of 9.0, 32.0, and 50.3 MHz for the c -axis sound-wave propagation direction. These plots are representative of the data taken at each of these frequencies. These curves indicate that for each of the three frequencies investigated the entire temperature range $1.0 < t \leq 0.44$ was fitted very well with one slope, i. e., one 0-K limiting energy gap, $\Delta(\vec{q}, 0)$. The average values of $2\Delta(\vec{q}, 0)$ in units of kT_c are tabulated for each frequency in Table I. The stated error given with each value of $2\Delta(\vec{q}, 0)$ has been

estimated from the reproducibility of the energy gap from one data set to another. These values indicate that for sound propagating in the c -axis direction, the energy gap is frequency independent over the frequency range investigated.

Also tabulated in Table I are the extrapolated total electronic attenuation values α_e , in units of dB/cm for each of these three frequencies. These values of α_e are shown plotted as a function of frequency in Fig. 5, where the scatter in the extrapolated value is indicated by the error bars. Since this curve is linear in frequency, the Pippard theory indicates $ql > 1$. This is in agreement with the magnetoacoustically determined electron mean free path where it was determined that $ql > 6.8$ for $\vec{q} \parallel [0001]$ for all magnetic-field orientations and for all frequencies investigated.

2. Results for $\vec{q} \parallel [10\bar{1}0]$

Figure 6 summarizes the data for ultrasound propagating in the $[10\bar{1}0]$ direction for frequencies of 9.0, 31.5, 51.1, and 70.6 MHz. At the frequencies 31.5–70.6 MHz the data are represented by essentially a single frequency-independent energy gap. However, at the lowest ultrasonic frequency, 9.0 MHz, a slight lowering of the energy gap was noted with a tendency for the experimental data to deviate from a single slope.

Shown in Fig. 7 are the total electronic attenuation values α_e expressed as a function of frequency for $\vec{q} \parallel [10\bar{1}0]$. These data were found to be represented quite well by Eq. (1), where α' and l were

TABLE I. Effective energy gap $2\Delta(\vec{q}, 0)$ and apparent second gap $2\Delta^*(\vec{q}, 0)$ in units of kT_c as a function of frequency and crystallographic direction. Also given are the total electronic attenuation α_e in units of dB/cm and the average ql value at each frequency studied.

Average ql	Frequency (MHz)	α_e (dB/cm)	$2\Delta^*(\vec{q}, 0)$ (kT_c)	$2\Delta(\vec{q}, 0)$ (kT_c)
$\vec{q} \parallel [0001]$				
180	9.0	4.5	...	3.00 ± 0.10
650	32.0	19.8	...	3.00 ± 0.10
1010	50.3	33.0	...	3.02 ± 0.10
$\vec{q} \parallel [10\bar{1}0]$				
0.39	9.0	0.3	3.48 ± 0.20	2.74 ± 0.10
1.15	31.5	1.8	...	2.78 ± 0.10
1.92	51.1	3.9	...	2.94 ± 0.20
2.69	70.6	6.4	...	2.82 ± 0.10
$\vec{q} \parallel [11\bar{2}0]$				
0.13	9.4	0.6	3.58 ± 0.20	2.96 ± 0.10
0.38	31.5	0.2	...	3.20 ± 0.10
0.64	53.0	4.4	4.66 ± 0.20	3.52 ± 0.10
0.90	70.6	6.5	4.80 ± 0.20	3.98 ± 0.10
1.15	90.5	7.3	5.00 ± 0.20	4.02 ± 0.20
1.41	110	6.9	4.42 ± 0.20	3.96 ± 0.20
1.67	130	6.2	...	3.76 ± 0.10
1.92	150	7.5	...	3.74 ± 0.10
2.18	170	9.2	...	3.80 ± 0.10

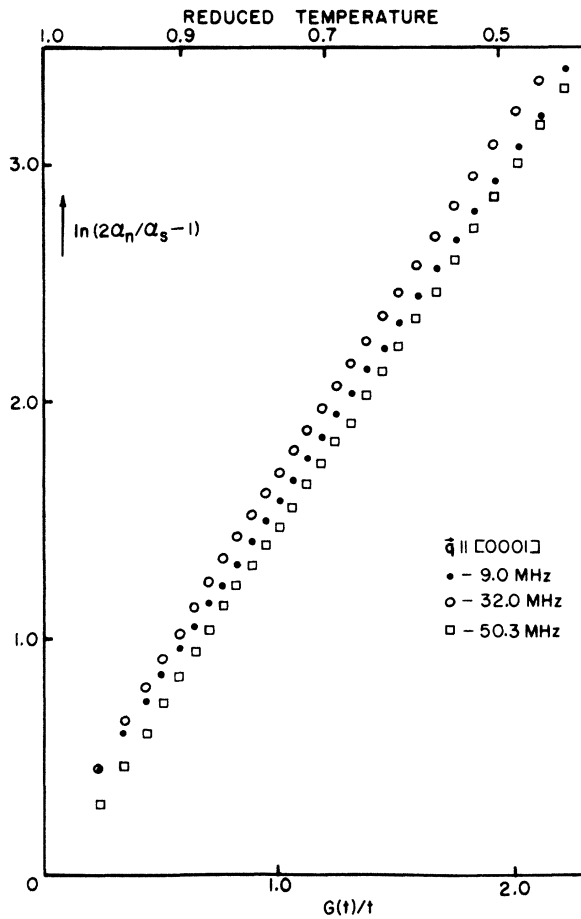


FIG. 4. Representations of $\ln(2\alpha_n/\alpha_s - 1)$ vs $G(t)/t$ at frequencies of 9.0, 32.0, and 50.3 MHz for longitudinal waves propagated in the [0001] direction.

adjustable parameters. The mean free path l which essentially determines the curvature since α' is just an amplitude factor, was determined to be 0.003 cm. Since this value is a complicated average over the "effective zone" on the Fermi

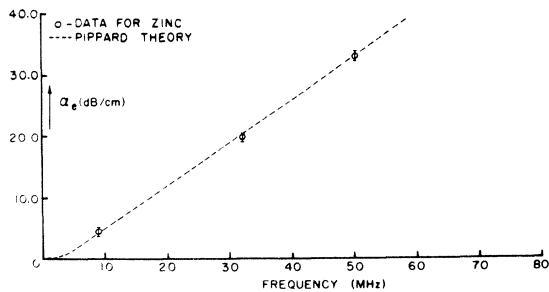


FIG. 5. Plot of the total electronic attenuation data α_e vs frequency for longitudinal waves propagated in the [0001] direction.

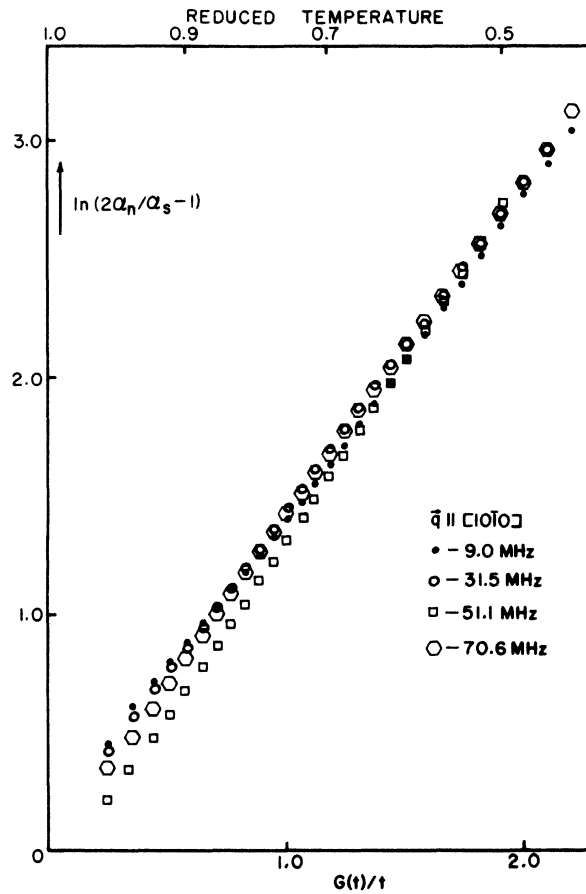


FIG. 6. Representations of $\ln(2\alpha_n/\alpha_s - 1)$ vs $G(t)/t$ at frequencies of 9.0, 31.5, 51.1, and 70.6 MHz for longitudinal waves propagated in the [1010] direction.

surface, a direct comparison with the magnetoacoustic data is difficult. However, a value of 0.006 cm, which is consistent with the value obtained from the Pippard theory, was estimated from the magnetoacoustic data.

3. Results for $\vec{q} \parallel [11\bar{2}0]$

Representative data for the crystallographic direction $[11\bar{2}0]$ at the odd harmonic frequencies of 9.4–170 MHz are shown in Figs. 8 and 9. It is observed that for all ultrasonic frequencies below 130 MHz except 31.5 MHz, the data are represented best by two frequency-dependent 0-K energy gaps, i. e., one gap $\Delta(\vec{q}, 0)/kT_c$ in the lower temperature region where $0.88 \geq t \geq 0.44$, and another gap $\Delta^*(\vec{q}, 0)/kT_c$ in the higher temperature region where $0.98 \geq t \geq 0.88$. At and above 130 MHz the data are represented very well by a single frequency-independent 0-K energy gap.

The total electronic attenuation α_e expressed as a function of frequency is seen in Fig. 10. Again

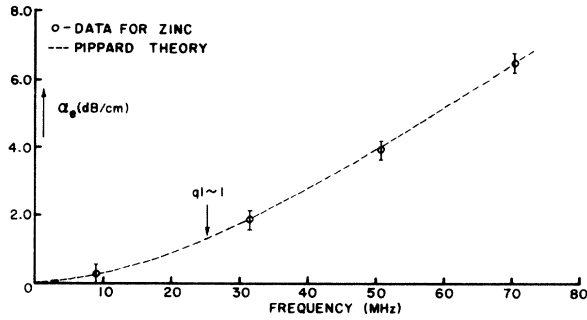


FIG. 7. Plot of the total electronic attenuation data α_e vs frequency for longitudinal waves propagated in the $[10\bar{1}0]$ direction.

the broken line represents the Pippard theory, where the data were analyzed in the same manner as discussed for $\vec{q} \parallel [10\bar{1}0]$. The only exception here is that the curve was fitted for the total electronic attenuation data above 110 MHz and then extended below 110 MHz using Eq. (1). The aver-

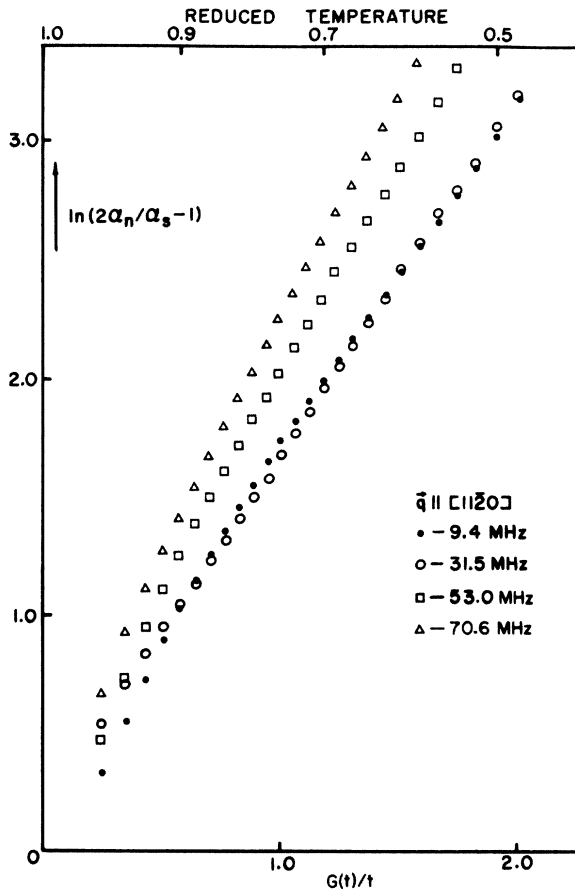


FIG. 8. Representations of $\ln(2\alpha_n/\alpha_s - 1)$ vs $G(t)/t$ at frequencies of 9.4, 31.5, 53.0, and 70.6 MHz for longitudinal waves propagated in the $[11\bar{2}0]$ direction.

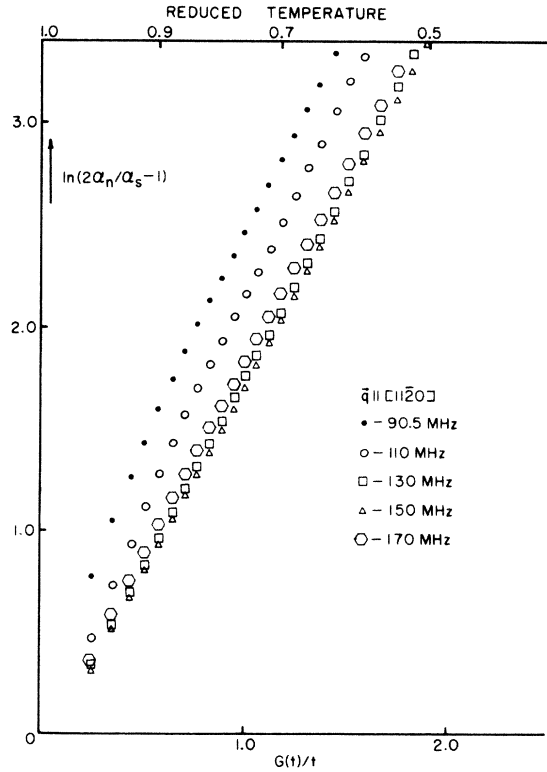


FIG. 9. Representations of $\ln(2\alpha_n/\alpha_s - 1)$ vs $G(t)/t$ at frequencies of 90.5, 110, 130, 150, and 170 MHz for longitudinal waves propagated in the $[11\bar{2}0]$ direction.

age mean free path determined in this manner was 0.001 cm, which is again found to be consistent with the value of 0.005 cm estimated from the magnetoacoustic results.

From the magnetoacoustic analysis for $\vec{q} \parallel [11\bar{2}0]$, it is observed that the "hump" in the α_e versus frequency curve (Fig. 10) occurs in the frequency range where the effective ql value is a complicated average of ql values for $ql \geq 1$ and $ql \leq 1$. This analysis also indicates that for all parts of the "effective zone," $ql > 1$ when $\nu \geq 130$ MHz and $ql < 1$ when $\nu \leq 30$ MHz. Hence, the hump appears in the frequency range where the "effective zone" is making its transition from the $ql < 1$ regime to the $ql > 1$ regime, and this range is seen to span approximately 100 MHz. Therefore credence is given to the magnetoacoustic analysis in that it apparently indicates the range of sound-wave frequencies for which selectivity and the rate of change of selectivity on the "effective zone" are important. It is also the contention of these authors that this analysis indicates that the mean free paths measured in the magnetoacoustic case are essentially the same as those measured in the zero-field case, i. e., those arrived at from the Pippard theory, except that the zero-field case

TABLE II. Previous ultrasonic determinations of the superconducting energy gap in pure zinc.

Authors	Direction of propagation	l (μm) 5%	$2\Delta(\vec{q}, 0)$ (kT_c)
Lea and Dobbs (Ref. 1)	$[11\bar{2}0]$	79.0	3.64 ± 0.1
	$[10\bar{1}0]$	29.6	3.79 ± 0.1
	$[0001]$	17.1	3.41 ± 0.1
Bohm and Horwitz (Ref. 2)	$[11\bar{2}0]$...	3.8 ± 0.2
	$[10\bar{1}0]$...	3.4 ± 0.2
Goncz and Neighbors (Ref. 3)	$[0001]$...	3.2 ± 0.4

will be some complicated average over the "effective zone" of those measured magnetoacoustically. However, it is not to be implied that when portions of the "effective zone" have $ql \sim 1$ that deviations from the free-electron model or a hump in $\alpha(\nu)$ will occur. As pertaining to Zn, this will be discussed further in Sec. V. It should also be noted that the hump cannot be due to dislocation-phonon interactions since the interactions of sound waves with dislocations cause the total electronic attenuation to have an apparent decrease in magnitude, not an increase in magnitude, as observed

in Fig. 10.

V. CONCLUSIONS

The results obtained from this investigation indicate that as the ql product becomes greater than 1, the effective 0-K energy gap tends toward a single limiting frequency-independent value. Also, when all parts of the effective zone have $ql > 1$, the description of ultrasonic attenuation developed by Pippard for the normal state using a simple free-electron model appears quite adequate. Therefore, the energy gaps corresponding to the case where all parts of the effective zone have $ql > 1$ are interpreted as representing the frequency-independent energy gaps predicted by BCS. From Table I these limiting energy gaps $2\Delta(\vec{q}, 0)$ are seen to be 3.00 ± 0.10 , 2.82 ± 0.10 , and 3.80 ± 0.10 in units of kT_c for ultrasound propagated parallel to the $[0001]$, $[10\bar{1}0]$, and $[11\bar{2}0]$ crystallographic directions, respectively.

These results indicate that the superconducting energy gap in zinc is highly anisotropic. Using the isotropic BCS value of $1.76kT_c$ as the average 0-K energy gap $\Delta(0)$, the calculated anisotropy for the limiting energy gaps in zinc is approximately 20% ($\langle a^2 \rangle \approx 0.040$). Given in Table II are the results of previous ultrasonic-attenuation investiga-

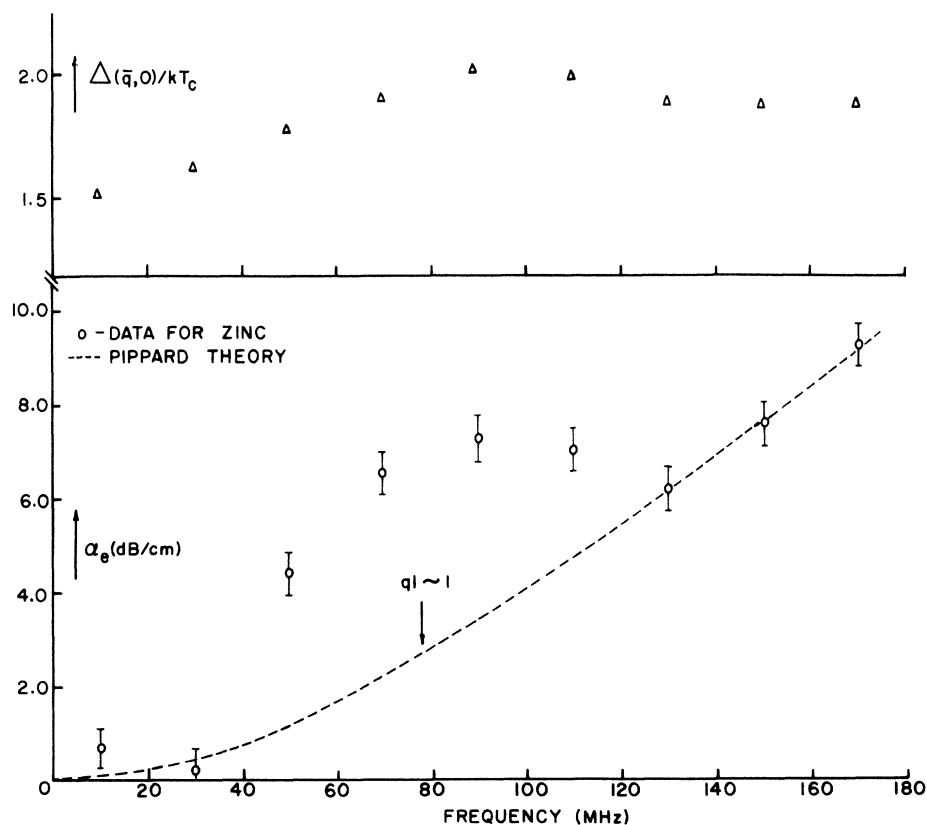


FIG. 10. Plot of the total electronic attenuation data α_e and the effective 0-K energy-gap data $\Delta(\vec{q}, 0)$ vs frequency for longitudinal waves propagated in the $[11\bar{2}0]$ direction.

tions in superconducting zinc. These energy-gap values indicate an anisotropy no larger than $\pm 5\%$. The discrepancy between the previous investigations and the present work lies mainly in the value of the energy gap obtained for $\vec{q} \parallel [10\bar{1}0]$. Without access to their data and experimental method (both Lea and Dobbs¹ and Bohm and Horwitz² used adiabatic demagnetization refrigerators), it is difficult to speculate as to the cause of this large discrepancy in anisotropy. However, as previously mentioned, the thermal-conductivity data of Zavaritskii,⁴ the microwave-absorption data of Evans *et al.*,⁶ the specific-heat data of Duclausoares and Cheeke,⁵ and the recent critical-magnetic-field data of Gubser and Cox⁹ all indicate an anisotropy of about the same magnitude as reported in this investigation.

Zavaritskii's measurements on the anisotropic electronic thermal conductivity utilized a prolate spheroidal model in calculating the energy gap as a function of direction. His results indicate a maximum gap of $3.5kT_c$ along the c axis and a minimum gap of $2.4kT_c$ perpendicular to the c axis. The anisotropic microwave-absorption measurements of Evans *et al.* indicate that most of the Fermi surface is associated with an energy gap of $(3.0 \pm 0.1)kT_c$ while the energy gap near the c axis is approximately $(4.0 \pm 0.2)kT_c$. The value they assign to the energy gap near the c axis was uncertain due to the effects of the surface on their results. The surface caused, in general, a large-angle scattering of the electrons which mixed the energy gaps from two different directions.

Since the "effective zone" in the ultrasonic-attenuation measurements is perpendicular to the sound-wave propagation direction, the gap found near the c axis in the thermal-conductivity and microwave-absorption measurements corresponds to the gap measured ultrasonically for either $\vec{q} \parallel [10\bar{1}0]$ or $\vec{q} \parallel [11\bar{2}0]$. Consequently, examining the results of the present work, it is concluded that the maximum gap measured by Zavaritskii and the large gap measured by Evans *et al.* are the same gap measured ultrasonically in this investigation for $\vec{q} \parallel [11\bar{2}0]$. Also, the gap indicated for most of the Fermi surface by Evans *et al.* of $(3.0 \pm 0.1)kT_c$ is found to be consistent with the results in this investigation of $(3.00 \pm 0.10)kT_c$ and $(2.82 \pm 0.10)kT_c$ for $\vec{q} \parallel [0001]$ and $\vec{q} \parallel [10\bar{1}0]$, respectively.

Other determinations of the anisotropic energy gap in zinc from bulk measurements have been reported for specific-heat measurements by Duclausoares and Cheeke⁶ and recently for critical-magnetic-field measurements by Gubser and Cox.⁹ They reported anisotropies of $\sim 15\%$ ($\langle a^2 \rangle = 0.020$) and $\sim 17\%$ ($\langle a^2 \rangle = 0.03$), respectively.

Since Eq. (1) was developed using a free-electron model, the hump observed in the electronic-

attenuation data for $\vec{q} \parallel [11\bar{2}0]$ possibly indicates a strong deviation in zinc from the free-electron model for the "effective zone" associated with $\vec{q} \parallel [11\bar{2}0]$. That is to say, for a particular "effective zone" as expressed by Eq. (7), the selectivity of the electron-phonon interaction is strongly influenced by the shape of the Fermi surface in that zone. Thus for a very complicated Fermi surface such as that of zinc²⁹ (six sheets), deviations from the free-electron model as expressed by Eq. (1) can be expected to arise from the topology of the Fermi surface in any particular "effective zone." Considering the Fermi surface calculated by Stark and Falicov²⁹, the "effective zone" for $\vec{q} \parallel [10\bar{1}0]$ should be nearly-free-electron-like since their calculation indicates that the so-called "butterflies" and "stars" of the third and fourth electron bands are raised well above the Fermi level and thus are void of electron states. Therefore the "effective zone" associated with $\vec{q} \parallel [10\bar{1}0]$ is essentially on the nearly-free-electron-like "lens" centered at the symmetry point Γ . The frequency dependence of the electronic attenuation for $\vec{q} \parallel [10\bar{1}0]$ illustrated in Fig. 7 tends to support this interpretation. For $\vec{q} \parallel [11\bar{2}0]$, however, the "effective zone" includes portions of the Fermi surface which are not free-electron-like. This character is attributed to the dominant contribution of the outer d -shell electrons of the ion core to the potential in the vicinity of the K - H line in the Brillouin zone. Thus for $ql \sim 1$, deviations from Eq. (1) can be expected, since not only is the rate of change of selectivity great for the "effective zone" associated with $\vec{q} \parallel [11\bar{2}0]$ as indicated by Eq. (7), but also, as suggested by the data reported by these authors, the electron-phonon interaction is much more sensitive to the topology of the Fermi surface which possesses a non-free-electron-like character. For $\vec{q} \parallel [0001]$, $ql \gg 1$ for all frequencies investigated. Therefore, according to the Pippard theory¹⁸ and the preceding discussion, the dependence of the electronic attenuation should be a linear function of frequency [Eq. (2)]. This dependence is illustrated in Fig. 5.

As previously discussed, Eq. (7) also suggests that for an anisotropic superconductor the effective energy gap might show a dependence on ql for the lower ultrasonic frequencies. As the sound wave interacts with a larger portion of the Fermi surface (lower ql values), the effective energy gap will represent a weighted average of the gap anisotropy for that "effective zone." Then as $ql \rightarrow \infty$ the dependence on ql should disappear since Eq. (7) indicates that the "effective zone" becomes highly selective for $ql > 1$. This was essentially the dependence observed in the $[10\bar{1}0]$ and $[11\bar{2}0]$ crystallographic directions. This dependence was

not observed in the c -axis direction since $q \gg 1$ at all frequencies studied.

As was the case for the hump in the frequency dependence in the electronic attenuation for $\vec{q} \parallel [11\bar{2}0]$, the effective energy gap exhibits essentially the same frequency dependence (Fig. 1), and it is again attributed to the topology of the Fermi surface on the "effective zone" for $ql \sim 1$. This anomaly in the frequency dependence is expected since at the sound-wave frequencies (phonon energies) studied in the present work, the electronic attenuation of the sound waves in the superconducting state is entirely due to the electron-phonon interaction with unpaired electrons. Thus it is expected that the effective energy gap should exhibit essentially the same frequency dependence as the electronic attenuation of the normal electrons.

The assignment of multiple energy gaps for sound propagating in the $[10\bar{1}0]$ and $[11\bar{2}0]$ directions is at most tentative since both the appearance of multiple gaps and the dependence of the gaps on ql in zinc probably arise due to anisotropy associated with each piece of Fermi surface studied and not to multiple energy surfaces found in the higher Brillouin zones. The justification for this statement lies in the fact that as all parts of the "effective zone" approach $ql > 1$ the apparent gap at

the higher reduced temperatures approaches the value of the gap at the lower reduced temperatures which has become frequency independent as expected from Eq. (7). This indicates that as the sound wave becomes more selective and interacts with a smaller portion of the Fermi surface, the energy gap associated with that portion becomes less anisotropic. If more than one gap were present for a specific region of k space, it would be expected that on the basis of multiple-band theory the gap at the higher reduced temperatures would reach a limiting value other than that found at the lower reduced temperatures as ql becomes greater than one. However, since both values are found to be the same, the appearance of multiple energy gaps in the data analysis is attributed to anisotropy with the greater rate of change of selectivity near $ql \sim 1$ associated with the "effective zone" for $\vec{q} \parallel [11\bar{2}0]$.

ACKNOWLEDGMENTS

The authors appreciate the assistance of Dr. W. O. Milligan, Director of Research for Robert A. Welch Foundation, Dr. R. Robbins, and Dr. S. G. O'Hara for stimulating discussions and assistance during the course of this work.

*Work supported by the Robert A. Welch Foundation.

¹M. J. Lea and E. R. Dobbs, *Phys. Lett. A* **27**, 556 (1968).

²H. V. Bohm and N. H. Horwitz, in *Proceedings of the Eighth International Conference on Low Temperature Physics* (Butterworths, London, 1963), p. 191.

³J. P. Goncz and J. R. Neighbors (private communications).

⁴N. V. Zavaritskiĭ, *Zh. Eksp. Teor. Fiz.* **39**, 1193 (1960) [*Sov. Phys.-JETP* **12**, 831 (1961)].

⁵H. A. Boorse, *Phys. Rev. Lett.* **2**, 391 (1959).

⁶E. Ducla-Soares and J. D. N. Cheeke, in *Proceedings of the Twelfth International Conference on Low Temperature Physics*, edited by E. Kanda (Academic Press of Japan, Tokyo, 1970), p. 305.

⁷D. Farrell, J. G. Park, and B. R. Coles, *Phys. Rev. Lett.* **13**, 328 (1964).

⁸J. B. Evans, M. P. Garfunkel, and D. A. Hays, *Phys. Rev. B* **1**, 3629 (1970).

⁹D. U. Gubser and J. E. Cox, *Phys. Rev. B* **7**, 4118 (1973).

¹⁰L. N. Cooper, *Phys. Rev. Lett.* **3**, 17 (1959).

¹¹Materials Research Corp., Orangeburg, New York.

¹²B. D. Cullity, *Elements of X-Ray Diffraction* (Addison-Wesley, Reading, Mass., 1957).

¹³R. Truell, C. Elbaum, and B. Chick, *Ultrasonic Methods in Solid State Physics* (Academic, New York,

1969).

¹⁴R. B. Hemphill, *Rev. Sci. Instrum.* **39**, 910 (1968).

¹⁵R. A. Robbins and B. J. Marshall, *J. Appl. Phys.* **42**, 2562 (1971).

¹⁶S. G. Sydoriak and T. R. Roberts, *Phys. Rev.* **106**, 175 (1957).

¹⁷J. R. Clement and E. H. Quinell, *Rev. Sci. Instrum.* **23**, 213 (1952).

¹⁸A. B. Pippard, *Philos. Mag.* **46**, 1104 (1955).

¹⁹J. Bardeen, L. N. Cooper, and J. R. Schrieffer, *Phys. Rev.* **108**, 1175 (1957).

²⁰T. Tsuneto, *Phys. Rev.* **121**, 402 (1961).

²¹B. Muhlschlegel, *Z. Phys.* **155**, 313 (1959).

²²J. R. Clem, *Ann. Phys. (N.Y.)* **50**, 268 (1966).

²³J. R. Leibowitz, *Phys. Rev.* **133**, A84 (1964).

²⁴R. W. Morse, *Prog. Cryog.* **1**, 211 (1959).

²⁵B. C. Deaton and J. D. Gavenda, *Phys. Rev.* **129**, 1990 (1963).

²⁶B. C. Deaton, *Phys. Rev.* **140**, A2051 (1965).

²⁷A. B. Pippard, *Proc. R. Soc. A* **257**, 165 (1960).

²⁸In the investigation of the mean free path in zinc by Deaton (Ref. 26), the crystallographic directions $[11\bar{2}0]$ and $[10\bar{1}0]$ were inadvertently reversed. This has been experimentally confirmed using the zinc specimen graciously loaned by Dr. Deaton.

²⁹R. W. Stark and L. M. Falicov, *Phys. Rev. Lett.* **19**, 795 (1967).